Lamellar Orientation and Corresponding Rheological Properties of Symmetric Diblock Copolymers under Steady Shear Flow

Kaifu Luo and Yuliang Yang*

Department of Macromolecular Science, Key Laboratory of Molecular Engineering of Polymers, SMEC, Fudan University, Shanghai 200433, China

Received May 22, 2001; Revised Manuscript Received January 6, 2002

ABSTRACT: The kinetics of lamellar orientation and rheological properties of symmetric diblock copolymers under steady shear flow using the time-dependent Ginzburg−Landau (TDGL) approach were studied. The simulation results show that a high shear rate can induce a perpendicular alignment for temperatures just below the order−disorder transition (ODT). On the other hand, a low shear rate induces initially mixed morphologies composed primarily of perpendicular and parallel orientations; eventually, the perpendicular alignment is transformed into a parallel alignment via undulation instability. On the contrary, with decreasing temperature, the high shear rate produces a parallel alignment, and the low shear rate induces a perpendicular alignment. The results also show that the reduced shear viscosity rapidly reaches a maximum at a reduced shear strain near one and then decreases. The first and second normal stress differences N_1 and N_2 are related to the lamellar alignment.

1. Introduction

Block copolymer melts have received much attention over the past years due to their ability to self-assemble into a wide variety of ordered microstructures, such as body-center-cubic spheres (BCC), hexagonally ordered cylinders (HEX), lamellae (LAM), and more complex bicontinuous double gyroid (G) depending on their degrees of polymerization (N), interaction parameter (χ), and fractional compositions (f).[1,2]

Current interest has turned toward understanding flow-induced alignment microstructures.[3,4] A particular focus has been the effect of flow on the lamellar phase. In the quiescent state, when the lamellar phase is entered by quenching from the isotropic melt, the ordered state consists of randomly oriented grains with concomitant defects. Such "quenched" lamellar phases have local uniaxial order but lack long-ranged order and possess very unusual linear viscoelastic properties. A system under shear flow shows not only transitions between different morphologies but also transitions between different orientations of these morphologies with respect to the shear geometry. The "parallel alignment", i.e., lamellar normal is parallel to the velocity gradient direction, and the "perpendicular alignment", i.e., lamellar normal is parallel to the vortex direction, have been induced in the bulk by large-amplitude oscillatory shear (LAOS) in both poly(styrene-*b*-ethylene) (PS−PI) type and poly(ethylene−propylene-*b*-ethylethylene) (PEP−PEE) type.[5−21] Generally speaking, in symmetric PS−PI diblock melts, a parallel alignment is favored at high frequencies.[10,11] On the contrary, a perpendicular alignment is favored at low frequencies.[5−7] At a still lower frequency, Zhang et al.[14,16,17] have found the existence of an additional parallel alignment regime; however, others have not found such a regime in PS−PI melts.[7,11] This discrepancy may be due to the different thermal histories during sample preparation. Additionally, Zhang and Wiesner[15] have identified a "transverse alignment", in which the lamellar normal is parallel to the velocity direction, well below the ODT in symmetric PS−PI diblock copolymer melts under LAOS. The experiments were performed well into the entanglement plateau, and the authors suggested that topological constraints were responsible for this new result. LAOS has also been used to induce mixed bulk morphologies, composed primarily of parallel and perpendicular orientations in a PS−PI system[22] and parallel-transverse biaxial orientations in PS−PI and PS−PEP systems.[8,9,23,24]

On the other hand, few experimental studies have been performed under steady shear flow, and the pathway of lamellar alignment is not understood very well. Balsara et al.[25] reported that the mixed orientation state with some perpendicular as well as parallel characters in a concentrated PS−PI block copolymer solution in a neutral solvent under steady shear flow was observed near the quiescent ODT. For the same system, Zryd and Burghard[26] found that, in steady-shear-flow experiments well bellow ODT, a perpendicular alignment appeared at low shear rates and a parallel alignment emerged at high shear rates. They also found that as the temperature is increased, the degree of perpendicular alignment obtained at low reduced shear rates decreases. Kitade et al.[27] reported that the steady shear flow exerted almost no effect on the microdomain structure for lower molecular weight symmetric poly(styrene-d_8-*b*-2-vinylpyridine) solution in a common solvent for both block components. For a solution of higher molecular weight sample, lamella orientation induced by shear flow was observed. For temperature $T < T_c$ (a characteristic temperature), at shear rate $\dot{\gamma} < \dot{\gamma}_c$ (a characteristic shear rate) the lamellae with normals lying in the shear gradient−vorticity plane exist. With increasing $\dot{\gamma}$, the perpendicular orientation increases, and eventually it becomes dominant at $\dot{\gamma} \geq \dot{\gamma}_c$. On the other hand, for $T > T_c$, at $\dot{\gamma} < \dot{\gamma}_c$ the isotropic scattering is observed, while the perpendicular orientation becomes dominant at $\dot{\gamma} \geq \dot{\gamma}_c$. A region where the parallel orientation is dominant was not observed. It should be pointed out that the results for temperature $T < T_c$ are different from those of Zryd and Burghard's

* To whom correspondence should be addressed. E-mail: ylyang@srcap.stc.sh.cn.

10.1021/ma010889j CCC: $22.00
Published on Web 03/28/2002

experiments well below ODT. The discrepancies may be due to different diblock copolymer types, molecular weights, and the experimental conditions.

On the theoretical side, by applying a self-consistent Hartree approximation to the nonequilibrated system, Cates and Milner[28] evaluated the role of steady shear in the isotropic−lamella transition. They first formulated the concept that the attenuation of the fluctuation field induced by shear drives the system toward the mean-field limit, and eventually the disordered copolymer melts become less stable, which results in an apparent increase of the ODT temperature. Later, Fredrickson[29] modified the theory of Cates and Milner to incorporate mechanical contrast between blocks in lamellar melt. In particular, perpendicular lamellae were predicted to be stable just below ODT under strong shear conditions, while parallel lamellas are favored under conditions of weak shear flow or lower temperatures.

It can be clearly seen that the above experimental results are not completely followed by the predictions of Fredrickson theory.[29] Especially the theory cannot predict the occurrence of the mixed orientation state. Therefore, a numerical simulation is a better approach to determine the patterns formed during of microphase separation in diblock copolymers under steady shear flow. Previously, numerical simulations of polymer system under shear flow have been carried out for lamellar and cylindrical phase in two-dimensional (2D) systems. We must point out that the simulation carried out in 2D cannot determine the morphology formed accurately. To our knowledge, very few simulations of copolymer morphology in three-dimensional (3D) system under shear flows have been reported.[30,31] Recently, Zvelindovsky et al.[31] have reported 3D density-functional calculations for lamellar phase. The most stable perpendicular lamellar ordering is observed in their simulations.

In addition, correlation between the nonlinear rheological properties and microstructural development of block copolymer under a shear flow is a challenging topic. Ohta et al.[32,33] presented numerical simulation data for the regular hexagonal phase subjected to strong cross-axis shear. The scheme involves developing numerical solutions of the standard time-dependent Ginzburg−Landau equation. Much remains to be done in this area.

In this paper, we use the time-dependent Ginzburg−Landau (TDGL) approach with Ohta and Kawasaki free energy[34] to investigate the kinetics of lamellar orientation and rheological properties of diblock copolymers under a simple shear flow in 3D. The organization of this paper is as follows. The models and algorithm are introduced in section 2. Section 3 presents the simulation results and discussions. Finally, the conclusions are drawn in section 4.

2. Models and Algorithm

To be concrete, we consider A−B diblock copolymers as the context. The appropriate order parameter is $\psi(\mathbf{r}) = 2(f - \phi_A(\mathbf{r})) = \phi_B(\mathbf{r}) - \phi_A(\mathbf{r}) - (1 - 2f)$, where $\phi_A(\mathbf{r})$ and $\phi_B(\mathbf{r})$ are respectively the local volume fraction of A and B monomers, and f is the fraction of A monomers in the diblock. The kinetics and morphological evolution are described, in the spirit of linear irreversible thermodynamics, by the TDGL equation for diffusive field coupled with an external velocity field, which can be written as[35]

$$\frac{\partial\psi(\mathbf{r},t)}{\partial t} + \mathbf{v}\cdot\nabla\psi(\mathbf{r},t) = M\nabla^2\frac{\delta F[\psi(\mathbf{r},t)]}{\delta\psi(\mathbf{r},t)} + \eta(\mathbf{r},t) \quad (1)$$

where we have used the fact that $\psi(\mathbf{r})$ is a conserved order parameter. In eq 1, M is a mobility coefficient, which is assumed to be a constant; $\mathbf{v}$ is an external velocity field describing shear flow profile

$$\mathbf{v} = \dot{\gamma} y \mathbf{e}_x \quad (2)$$

where $\dot{\gamma}$ is the shear rate and $\mathbf{e}_x$ is the unit vector in the x direction; and $\eta(\mathbf{r},t)$ is a Gaussian white noise, representing thermal fluctuation, with mean zero and correlation

$$\langle\eta(\mathbf{r},t)\,\eta(\mathbf{r}',t)\rangle = -2k_BTM\nabla^2\delta(\mathbf{r} - \mathbf{r}')\,\delta(t - t') \quad (3)$$

where T is the temperature of the fluid and $\langle ... \rangle$ denotes the ensemble average. As a minimal model, any hydrodynamics effects and possible nonlocality in the mobility coefficient are ignored. The thermal noise is also neglected in this simulation, as its effects are not crucial in the late stage of the microphase separation.

The equilibrium free energy function, consisting of short-range and long-range interaction terms, is written as[36−38]

$$F[\psi(\mathbf{r})] = \int d\mathbf{r}\left[f(\psi) + \frac{D}{2}\left|\nabla\psi\right|^2\right] + \frac{\alpha}{2}\int d\mathbf{r}\int d\mathbf{r}'\,G(\mathbf{r} - \mathbf{r}')\,\psi(\mathbf{r})\,\psi(\mathbf{r}') \quad (4)$$

where $f(\psi)$ reads

$$f(\psi) = \left[-\frac{a}{2} + \frac{b}{2}(1 - 2f)^2\right]\psi(\mathbf{r})^2 + \frac{v}{3}(1 - 2f)\psi(\mathbf{r})^3 + \frac{u}{4}\psi(\mathbf{r})^4 \quad (5)$$

The second term in eq 4 represents the long-range interaction, which arises from the connectivity of the two blocks and is typical of an amphiphilic system. The Green's function $G(\mathbf{r} - \mathbf{r}')$ satisfies $\nabla^2G(\mathbf{r} - \mathbf{r}') = -\delta(\mathbf{r} - \mathbf{r}')$. a is related to the distance from the order−disorder transition temperature, and the coefficients b, v, u, D, and α are phenomenological parameters.

In the following, we will focus our discussion on the symmetric diblock copolymers, so $f(\psi)$ becomes

$$f(\psi) = -\frac{a}{2}\psi(\mathbf{r})^2 + \frac{u}{4}\psi(\mathbf{r})^4 \quad (6)$$

Thus, the free energy defined in eq 4 becomes Otha and Kawasaki's free energy.[32] We must point out that the parameters a, D, and α can be related to molecular characteristics. According to Ohta and Kawasaki theory, a, D, and α are given in terms of the degree of polymerization N, the segments length σ, and the Flory−Huggins parameter χ as[32]

$$a = \frac{1}{N}(2\chi N - 7.2), \quad D = \frac{\sigma^2}{3}, \quad \alpha = \frac{144}{N^2\sigma^2} \quad (7)$$

So eq 1 can be written as

$$\frac{\partial\psi(\mathbf{r},t)}{\partial t} + \dot{\gamma} y \frac{\partial\psi(\mathbf{r},t)}{\partial x} = M\nabla^2(-a\psi + u\psi^3 - D\nabla^2\psi) - M\alpha\psi \quad (8)$$

With the substitution of the dimensionless variables

$$\mathbf{r}' = \mathbf{r}/\sqrt{D/a}, \quad \tau = t/(D/Ma^2), \quad \Psi(\mathbf{r}',\tau) = \psi(\mathbf{r},t)/\sqrt{a/u} \quad (9)$$

eq 8 becomes

$$\frac{\partial\Psi(\mathbf{r}',\tau)}{\partial\tau} + \frac{D\dot{\gamma}y'}{Ma^2}\frac{\partial\Psi(\mathbf{r}',\tau)}{\partial x'} = \nabla^2(-\Psi + \Psi^3 - \nabla^2\Psi) - \frac{D\alpha}{a^2}\Psi \quad (10)$$

Inserting eq 7 into eq 10, we obtain

$$\frac{\partial\Psi(\mathbf{r}',\tau)}{\partial\tau} + Sy'\frac{\partial\Psi(\mathbf{r}',\tau)}{\partial x'} = \nabla^2(-\Psi + \Psi^3 - \nabla^2\Psi) - \alpha'\Psi \quad (11)$$

where reduced shear rate $S = D\dot{\gamma}/Ma^2 = DN^2\dot{\gamma}/[M(2\chi N - 7.2)^2]$, and $\alpha' = D\alpha/a^2 = 48/[(2\chi N - 7.2)^2]$. For the symmetric diblock copolymers in a static state, the order−disorder transition takes place when $(\chi N)_c = 10.5$. Therefore, we have $\alpha'_c = 0.252 \approx {}^1/_4$.

Equation 11 is numerically solved by using the cell dynamical scheme (CDS) proposed by Puri and Oono.[39,40] In the 3D CDS, the system is discretized on a $L \times L \times L$ cubic lattice of cell size a_0, and the order parameter for each cell is defined as $\Psi(\mathbf{n},\tau)$, where $\mathbf{n} = (n_x, n_y, n_z)$ is the lattice position. n_x, n_y, and n_z are integers between 1 and L. The Laplacian in CDS is approximated by

$$\nabla^2\Psi(\mathbf{n}) = \frac{1}{a_0^2}(\langle\langle\Psi(\mathbf{n})\rangle\rangle - \Psi(\mathbf{n})) \quad (12)$$

where $\langle\langle\Psi(\mathbf{n})\rangle\rangle$ represents the following summation of $\Psi(\mathbf{n})$ for the nearest neighbors (n), the next-nearest neighbors (nn), and the next-next-nearest neighbors (nnn)[40]

$$\langle\langle\Psi(\mathbf{n})\rangle\rangle = B_1\sum_{\mathbf{n}=\mathrm{n}}\Psi(\mathbf{n}) + B_2\sum_{\mathbf{n}=\mathrm{nn}}\Psi(\mathbf{n}) + B_3\sum_{\mathbf{n}=\mathrm{nnn}}\Psi(\mathbf{n}) \quad (13)$$

where B_1, B_2, and B_3 are 6/80, 3/80, and 1/80 for the 3D system.

The time increment is set to be $\Delta\tau = 1$. The value of a_0^2 is fixed as 1.0. We should point out that, according to the simulations for $\Delta\tau = 0.01$, 0.1, 0.5, and 1, $\Delta\tau$ has no effect on the simulation results. Ignoring the thermal noise, then eq 11 is transformed to the following difference equation:

$$\Psi(\mathbf{n},\tau+1) = \Psi(\mathbf{n},\tau) - \frac{1}{2}Sy[\Psi(n_x+1,n_y,n_z,\tau) - \Psi(n_x-1,n_y,n_z,\tau)] + \langle\langle I(\mathbf{n},\tau)\rangle\rangle - I(\mathbf{n},\tau) - \alpha'\Psi(\mathbf{n},\tau) \quad (14)$$

with

$$I(\mathbf{n},\tau) = -\Psi(\mathbf{n},\tau) + \Psi(\mathbf{n},\tau)^3 - \{\langle\langle\Psi(\mathbf{n},\tau)\rangle\rangle - \Psi(\mathbf{n},\tau)\} \quad (15)$$

Our simulation was carried out on $L \times L \times L = 64 \times 64 \times 64$ three-dimensional cubic lattice. We have chosen the x-axis as the flow direction, the y-axis as the velocity gradient direction, and the z-axis as the vorticity axis. A shear periodic boundary condition proposed by Ohta et al.[35] has been applied to the y direction. With the shear strain γ, this boundary condition is written as

$$\psi(n_x,n_y,n_z,\tau) = \psi(n_x + N_xL + \gamma(\tau)N_yL,\ n_y + N_yL,\ n_z + N_zL) \quad (16)$$

where N_x, N_y, and N_z are arbitrary integers. An average was performed over four independent simulation runs with different set of random numbers for each initial state.

For phase-separating systems, the total stress consists of two parts: the contribution of chain relaxation and that of interfacial relaxation. Here, we are only interested in the morphological dependent stress resulted from the domain interface. Given the structure of the deformed morphology, the macroscopic stress due to interfacial relaxation can be calculated by the following formula derived by Kawasaki and Ohta,[41]

$$\frac{\sigma_{\alpha\beta}}{k_BT} = -\frac{D}{V}\int d\mathbf{r}\left(\frac{\partial\psi}{\partial r_\alpha}\right)\left(\frac{\partial\psi}{\partial r_\beta}\right) + \frac{\alpha}{V}\int d\mathbf{r}\int d\mathbf{r}'\, r_\beta\frac{\partial G(\mathbf{r})}{\partial r_\alpha}\psi\left(\mathbf{r}'+\frac{\mathbf{r}}{2}\right)\psi\left(\mathbf{r}'-\frac{\mathbf{r}}{2}\right), \quad \alpha,\beta = x,y,z \quad (17)$$

where k_BT is the Boltzmann constant times the absolute temperature, and D is the constant appeared in eq 4. In $\mathbf{q}$ space, according to eq 11, we obtain

$$\frac{\sigma_{\alpha\beta}}{k_BT} = -\frac{1}{L^5}\sum_{q\neq0}q_\alpha q_\beta\left(1 - \frac{\alpha'}{q^4}\right)|\Psi(\mathbf{q},\tau)|^2 \quad (18)$$

The first and second normal stress difference, N_1 and N_2, are defined as

$$\frac{N_1}{k_BT} = -\frac{\sigma_{xx} - \sigma_{yy}}{k_BT} \quad (19)$$

$$\frac{N_2}{k_BT} = -\frac{\sigma_{yy} - \sigma_{zz}}{k_BT} \quad (20)$$

The characteristic lengths at time τ in different directions, $R(x,\tau)$, $R(y,\tau)$, and $R(z,\tau)$, are calculated by[42−44]

$$R(\beta,\tau) = \left[\frac{\int d\mathbf{q}\ q_\beta^2 S(\mathbf{q},\tau)}{\int d\mathbf{q}\ S(\mathbf{q},\tau)}\right]^{-1/2} \quad \beta = x,y,z;\ q \in (-\pi,\pi) \quad (21)$$

where $S(\mathbf{q},\tau) = \langle\psi_{\mathbf{q}}(\tau)\,\psi_{-\mathbf{q}}(\tau)\rangle$ is the structure factor at time τ. Equation 21 is a second moment of the structure factor, and in some case it closely reflects an average interlamellar spacing for pattern of phase-separating diblock copolymers.

3. Simulation Results and Discussion

3.1. Domain Growth and Scattering Functions under Shear Flow. First, we fix the quench depth as $\chi N = 11.0$, which corresponds to temperature just below the ODT temperature. In this case $\alpha' \approx 0.22$ is near the critical point 0.252. The effects of shear rate on the

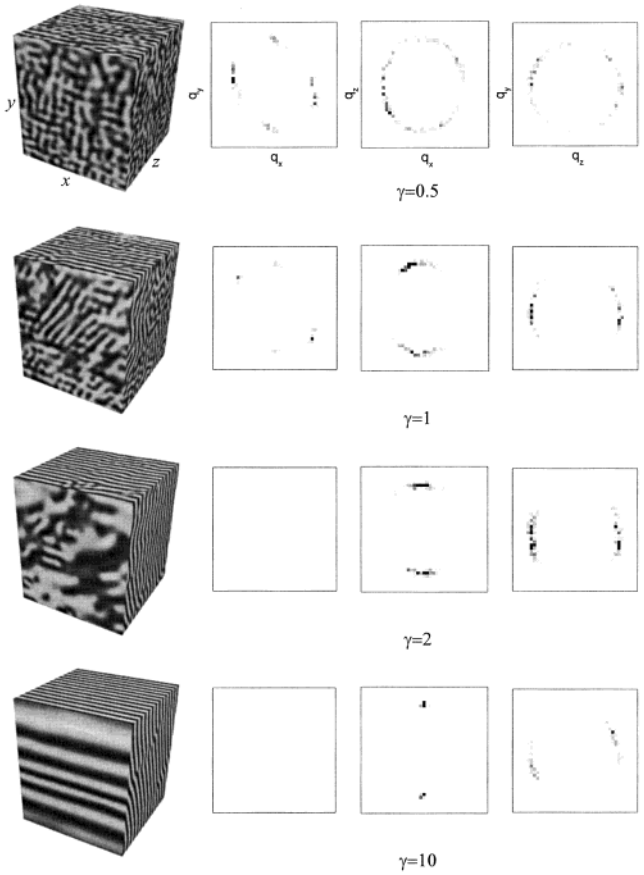

Figure 1. Simulated morphological evolution of the symmetric diblock copolymers with quench depth $\chi N = 11.0$ and the reduced shear rate $S = 0.001$.

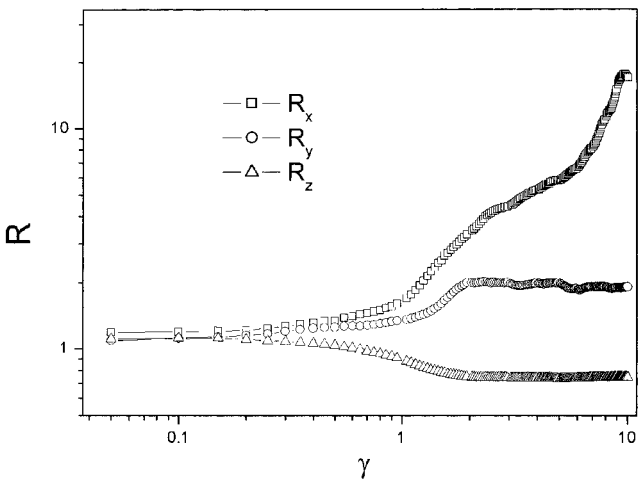

Figure 2. Evolution of the characteristic lengths (R_x, R_y, and R_z) for quench depth $\chi N = 11.0$ and the reduced shear rate $S = 0.001$ in the velocity, shear gradient, and vorticity directions.

pattern selection are investigated. The domain pattern and corresponding scattering pattern for different reduced shear rates $S = 0.001$ and 0.0002 are shown in Figures 1 and 3, respectively.

It can be clearly seen from Figure 1 that a global lamellar orientation appears with few defects. The orientation of the lamellar normal is perpendicular to the flow axis (x) and parallel to the vorticity axis (z) when the reduced shear strain $\gamma = S\tau \sim 10.0$. This kind of lamellar alignment is called "perpendicular alignment" in the literature. When reduced shear strain is

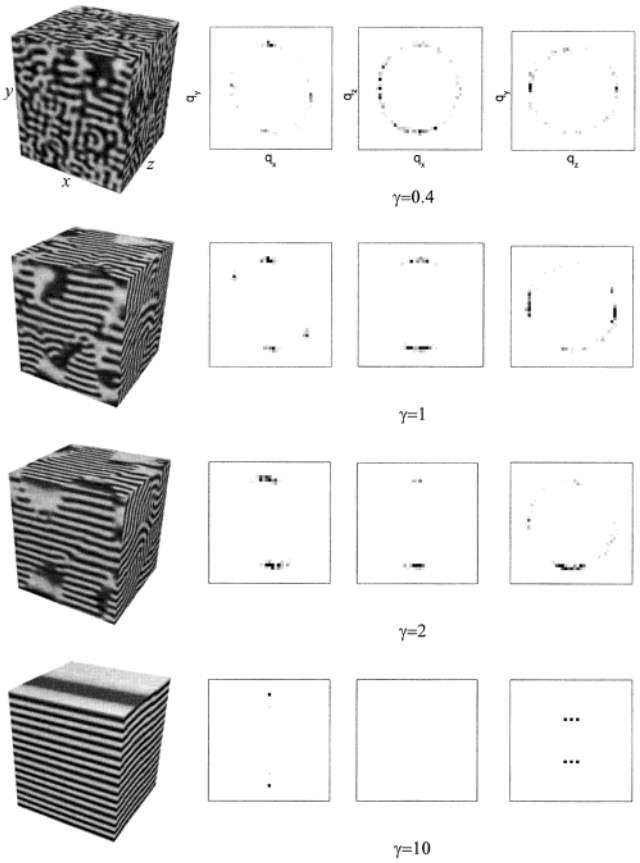

Figure 3. Simulated morphological evolution of the symmetric diblock copolymers with quench depth $\chi N = 11.0$ and the reduced shear rate $S = 0.0002$.

very low, i.e., $\gamma = 0.5$, the morphology is very like that of the polymer blends. The domains are only elongated slightly in the flow direction. In the velocity−shear gradient plane (q_x−q_y plane), the scattering function shows four peaks. In the velocity−vorticity plane (q_x−q_z plane) the scattering function is an elliptical ring. In the shear gradient−vorticity plane (q_y−q_z plane), the scattering is a standard spinodal ring. Like the phase separation of binary blends, in this plane the domains are less sensitive to shear flow. With the increase of the reduced shear strain, i.e., $\gamma = 1.0$, it can be seen that the pattern formed under a symmetry breaking field tends to be a perpendicular alignment with many defects emerging and elongating in the flow direction. The corresponding scattering functions confirmed the perpendicular lamella orientation. In the q_x−q_y plane, the scattering intensity decreases, but scattering function also has four very weak peaks. In the q_x−q_z plane, two broad strong peaks along vorticity direction are clearly seen. It indicates that the domain normals are oriented in the vorticity direction. At the same time, in the q_y−q_z plane, two strong peaks in the vorticity direction are also clear due to the same reason. Further increasing the reduced strain, i.e., $\gamma = 2.0$ and 10.0, leads to a perpendicular alignment with few defects. In the q_x−q_y plane, the scattering intensity is near zero. There are two stronger peaks along the vorticity direction in the q_x−q_z plane and q_y−q_z plane, respectively. Compared with $S = 0.0002$ shown in Figure 3, $S = 0.001$ has a much higher shear rate. We may conclude that a high shear rate can induce a perpendicular alignment in the regime of temperatures just below the ODT temperatures. In this regime, our predictions are in

agreement with other theoretical work[29] and the experimental results.[27]

The morphological evolution can be more quantitatively characterized by the characteristic lengths of $R(x,\tau)$, $R(y,\tau)$, and $R(z,\tau)$ defined in eq 21, which are shown in Figure 2. The evolution of these characteristic lengths describes the domain growth and the detailed pathways to the formation of different morphologies. It is seen from Figure 2 that $R(x,\tau)$ and $R(y,\tau)$ increase while $R(z,\tau)$ decreases with increase of a shear strain. Under the large reduced strain, $R(x,\tau)$ and $R(y,\tau)$ are much higher than $R(z,\tau)$. It should be mentioned that the value of $R(z,\tau)$ at the large reduced strain closely reflects the lamellar spacing. All these observations reveal that the perpendicular lamella alignment is achieved.

Now, we discuss the low reduced shear rate case, $S = 0.0002$. Figure 3 shows the evolution of the morphology and corresponding scattering function. When the reduced strain is very low, i.e., $\gamma = 0.4$, the morphology and corresponding scattering function are almost the same as those of the higher reduced shear rate case. However, when reduced shear strain $\gamma = 1$, a mixed morphology composed of perpendicular and parallel alignments is clearly seen. Correspondingly, the scattering function, in the q_x-q_y plane, has four strong peaks, and the two along the shear gradient direction are much stronger. In the q_x-q_z plane, compared with the case of higher reduced shear rate, two peaks along the vorticity direction are also observed. However, in the q_y-q_z plane, in addition to the two strong peaks along vorticity direction, the two weak peaks along the shear gradient direction can also be observed. The scattering pattern confirms the mixed lamella alignments. From the observed morphologies and the corresponding scattering patterns, it is clearly seen that the perpendicular alignment is dominant. With the increase of the reduced shear strain, i.e., $\gamma = 2$, the morphology still favors mixed alignments, although the fraction of the parallel alignment increases. However, instead of four peaks, we only observed two broad peaks along the shear gradient direction in the q_x-q_y plane and the scattering intensity increase. On the contrary, in the q_x-q_z plane, the intensity of two peaks along the vorticity direction decreases. Moreover, in the q_y-q_z plane, the four peaks are clearer, and we must point out that two peaks along shear gradient direction become stronger and other two peaks along vorticity direction become weaker. The morphology and corresponding scattering function indicate that in this stage the parallel alignment becomes predominant. When the reduced shear rate $\gamma = 10.0$, only the parallel alignment is observed. The scattering function in the q_x-q_y plane becomes two narrower strong peaks. Moreover, it also becomes two strong peaks along shear gradient direction instead of four peaks in the q_y-q_z plane. In the q_x-q_z plane, the scattering function tends to zero. Now, we can draw the conclusion that a low shear rate can induce a parallel alignment in the regime of temperatures just below the ODT temperature.

Figure 4 shows the evolution of the characteristic lengths of $R(x,\tau)$, $R(y,\tau)$, and $R(z,\tau)$. Compared with the evolution of the characteristic lengths for the high reduced-shear rate case shown in Figure 2, $R(x,\tau)$ increases rapidly with the increase of the shear strain. The $R(y,\tau)$ and $R(z,\tau)$ are almost unchanged until $\gamma = 2$, and then $R(y,\tau)$ decreases while $R(z,\tau)$ increases rapidly, reflecting the transition from mixed alignments to parallel alignment. At large strain, $R(x,\tau)$ and $R(z,\tau)$ are much larger than $R(y,\tau)$, which also closely reflects the lamellar spacing at large strain. All these observations reveal that the parallel lamella alignment is achieved.

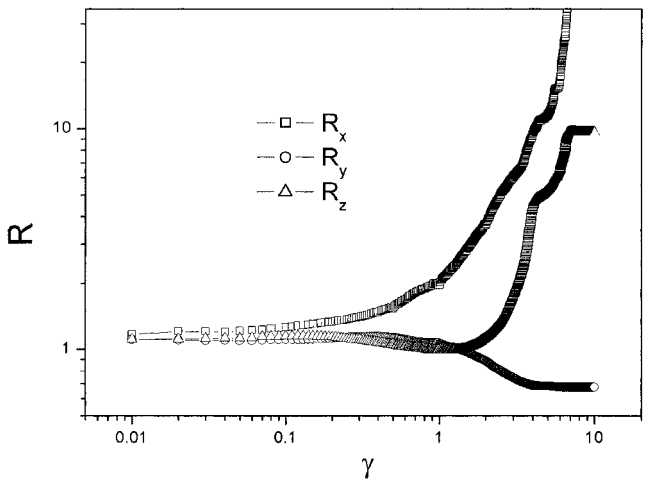

Figure 4. Evolution of the characteristic lengths (R_x, R_y, and R_z) for quench depth $\chi N = 11.0$ and the reduced shear rate $S = 0.0002$ in the velocity, shear gradient, and vorticity directions.

We must point out that a mixed morphology with lamellar normals lying in shear gradient−vorticity plane has been observed in the experiments (regime II; coexistent state of Balsara et al.).[25] Compared with our simulation results, we believe that the mixed morphology observed in the experiment could be an intermediate stage en route from the perpendicular alignment to parallel alignment. Compared with the Fredrickson theory,[29] the fact of forming parallel alignment is in agreement with the theory, but the theory did not predict the pathways of the formation of parallel alignment. Obviously, there is a "flipping" from the perpendicular to parallel alignments. However, what is the mechanism of this "flipping"?

To understand the mechanism of this "flipping", we studied a case with very low reduced shear rate, $S = 0.000\,05$. The results are shown in Figure 5. When $\gamma = 2.1$, the transition process from perpendicular to parallel alignments can be observed. Eventually, the perpendicular lamellae were transformed to parallel lamellae via undulation instability. To see more clearly, the morphologies in the shear gradient−vorticity plane ($y-z$ plane) are shown in Figure 6. The details of the transition can be described as follows. First, the perpendicular lamellae undulate and then reconnect along the direction perpendicular to flow direction to form a parallel alignment. It is well-known that the external shear field can cause the undulation instabilities. In a recent theoretical paper, Williams and MacKintosh[45] investigated the effect of oscillatory shear on the lamellar spacing in melts of symmetric diblock copolymers in the strong segregation limit. It was found that, before equilibrium is reached, the layers would show an undulational instability in the direction perpendicular to the velocity and the velocity gradient. Wang et al.[46] found that lamellae in the perpendicular orientation exhibit a shear-induced undulation instability. In this work, we have provided a basis for the mechanism from perpendicular to parallel alignments.

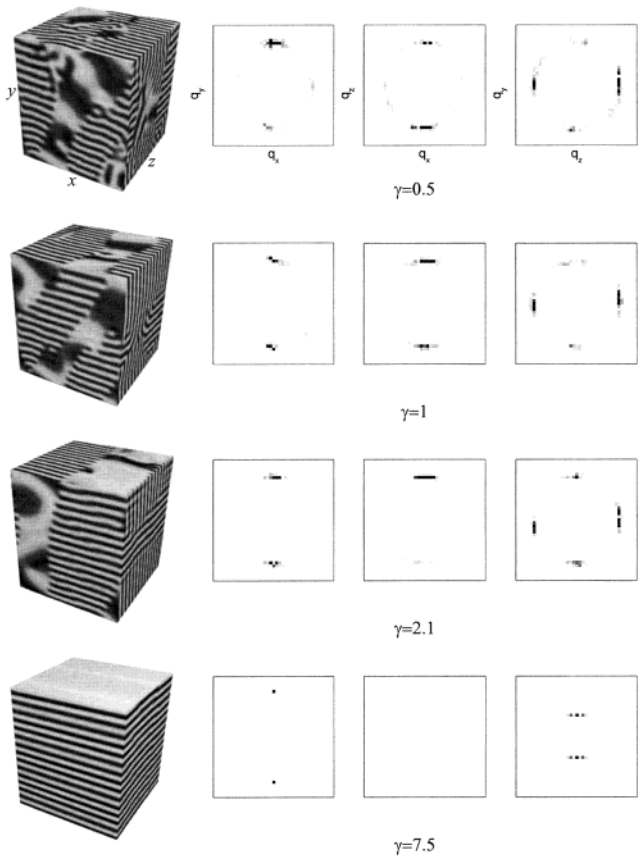

Figure 5. Simulated morphological evolution of the symmetric diblock copolymers with quench depth $\chi N = 11.0$ and the reduced shear rate $S = 0.000\ 05$.

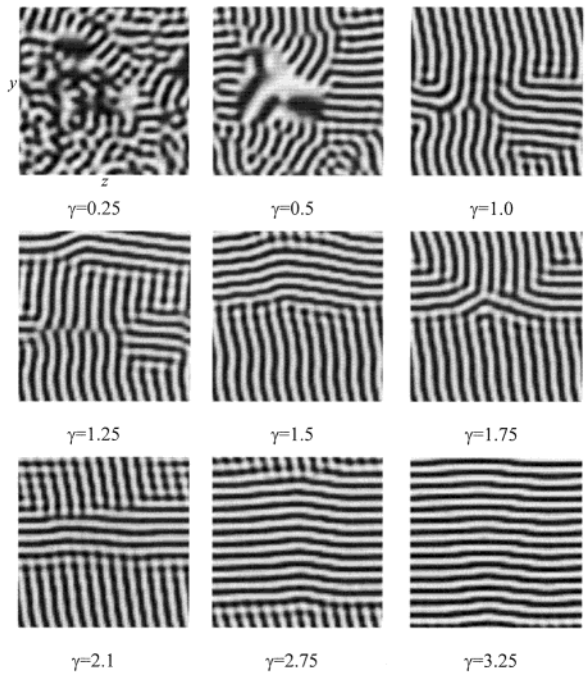

Figure 6. Simulated morphological evolution of the symmetric diblock copolymers in shear gradient−vorticity plane ($y-z$ plane) with quench depth $\chi N = 11.0$ and the reduced shear rate $S = 0.000\ 05$.

Now, we increase the quench depth as $\chi N = 15.0$. In this case $\alpha' \approx 0.09$ is much smaller than the critical point 0.252. The domain patterns and corresponding scattering patterns for different reduced shear rate,

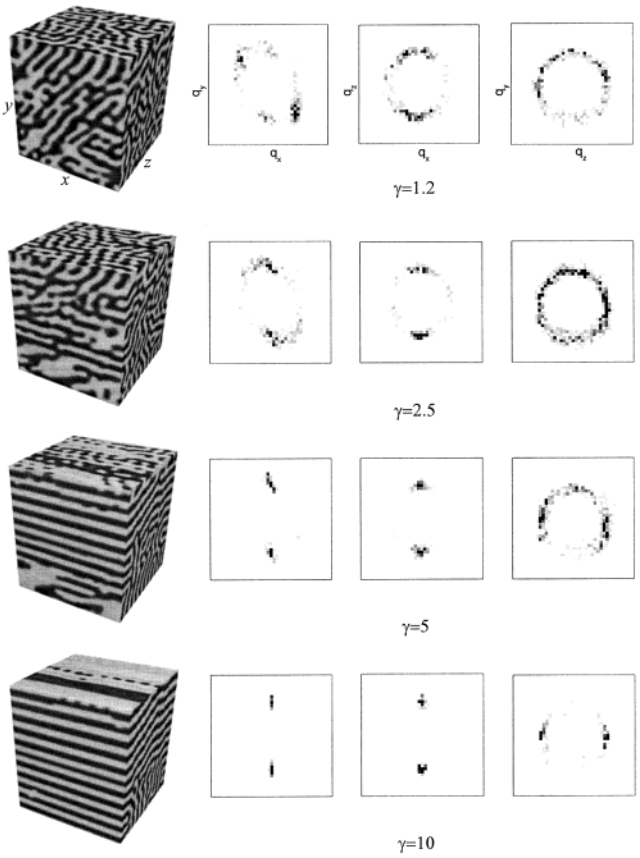

Figure 7. Simulated morphological evolution of the symmetric diblock copolymers with quench depth $\chi N = 15.0$ and the reduced shear rate $S = 0.0025$.

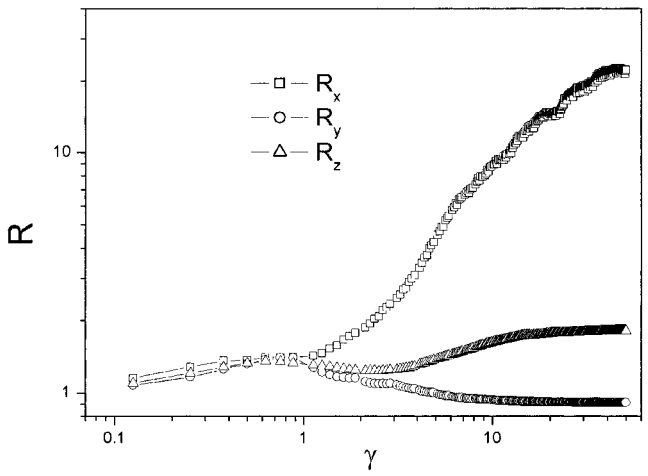

Figure 8. Evolution of the characteristic lengths (R_x, R_y, and R_z) for quench depth $\chi N = 15.0$ and the reduced shear rate $S = 0.0025$ in the velocity, shear gradient, and vorticity directions.

$S = 0.0025$ and 0.001, are shown in Figures 7 and 9, respectively. For the higher reduced shear rate case, $S = 0.0025$, we can see from Figure 7 that a parallel alignment with some defects is observed when the reduced shear strain is large. And a parallel alignment is formed directly, not experiencing a perpendicular alignment. Correspondingly, the evolution of the characteristic lengths of $R(x,\tau)$, $R(y,\tau)$, and $R(z,\tau)$ is shown in Figure 8, and it suggests the formation of a parallel alignment. On the contrary, for a low reduced shear rate, $S = 0.001$, Figure 9 shows that a perpendicular alignment occurs. Figure 10 shows the evolution of the

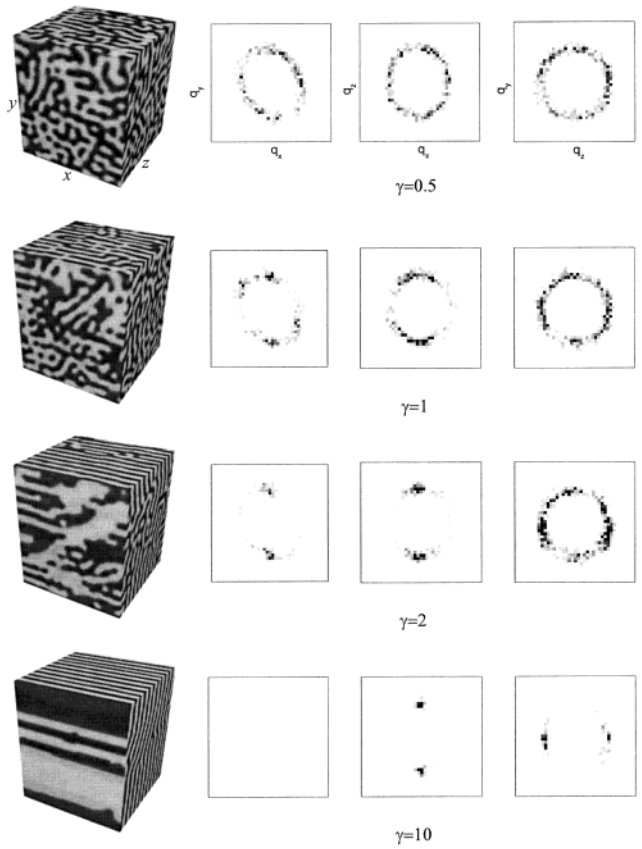

Figure 9. Simulated morphological evolution of the symmetric diblock copolymers with quench depth $\chi N = 15.0$ and the reduced shear rate $S = 0.001$.

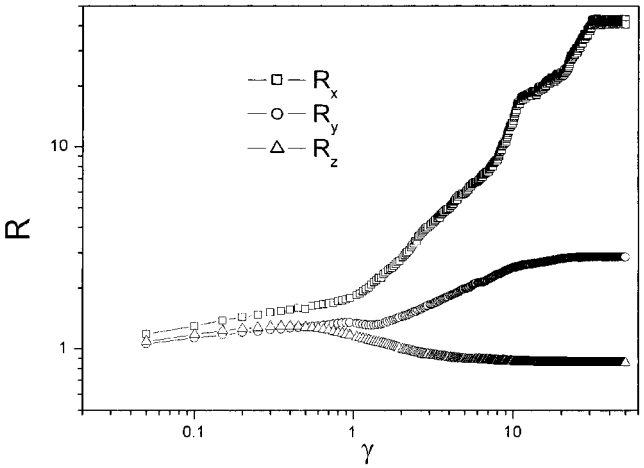

Figure 10. Evolution of the characteristic lengths (R_x, R_y, and R_z) for quench depth $\chi N = 15.0$ and the reduced shear rate $S = 0.001$ in the velocity, shear gradient, and vorticity directions.

characteristic lengths of $R(x,\tau)$, $R(y,\tau)$, and $R(z,\tau)$. It also indicates that a perpendicular alignment is observed. Therefore, we can draw the conclusion that an increase of the quenching depth leads to a parallel alignment under strong reduced shear rate and a perpendicular alignment under a low reduced shear rate. Fredrickson theory[29] predicted that lowering the temperature induced a parallel alignment. Obviously, the theory fails to explain our results for a low reduced shear rate case. In addition, we must point out our results are in agreement with the experimental results of Zryd and Burghard.[26]

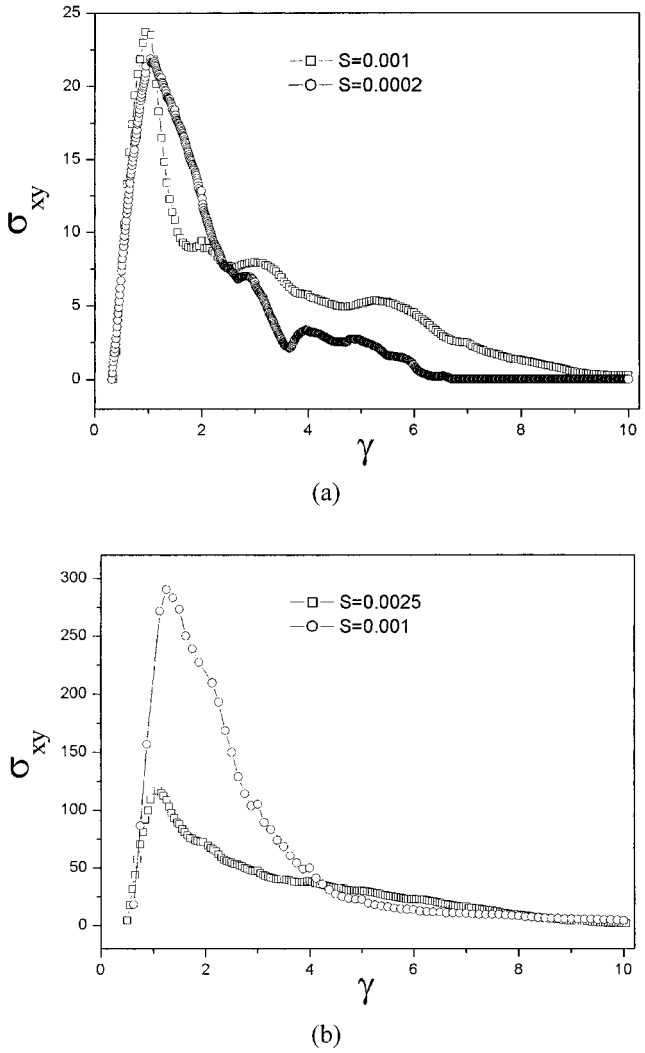

Figure 11. Reduced shear stress as a function of reduced strain for (a) $\chi N = 11.0$ and (b) $\chi N = 15.0$.

3.2. Rheological Properties Due to Deformed Domains. First, we discuss the reduced shear stress vs the reduced shear strain. Figure 11a shows the case $\chi N = 11.0$ for different reduced shear rate, $S = 0.001$ and 0.0002. Figure 11b shows the case $\chi N = 15.0$ for different reduced shear rate, $S = 0.0025$ and 0.001. It is clearly seen from Figure 10 that the reduced shear stress reaches a maximum rapidly at $\gamma \sim 1$ and then decreases. We must point out that the stress calculated from eq 18 only represents the interfacial contributions to the total stress. The volume of fraction of interface decreases after $\gamma \sim 1$, so the reduced shear strain is small at the large reduced shear strain. It is clearly seen from Figure 11a that the maximum of the shear stress for a high reduced shear rate is a bit larger than that for the low reduced shear rate. But we should note that the peak is wider for the case of low reduced shear rate, which is related to the formation of the mixed morphology. On the other hand, it is clearly seen from Figure 11b that the maximum of the shear stress for the high reduced shear rate is much larger than that for the low reduced shear rate. In addition, the maximum of the shear stress for $\chi N = 15.0$ is larger than that for the case of $\chi N = 11.0$.

Second, the reduced first and second normal stress difference N_1 and N_2 vs reduced shear strain were studied. Figure 12a,b shows the case $\chi N = 11.0$ for

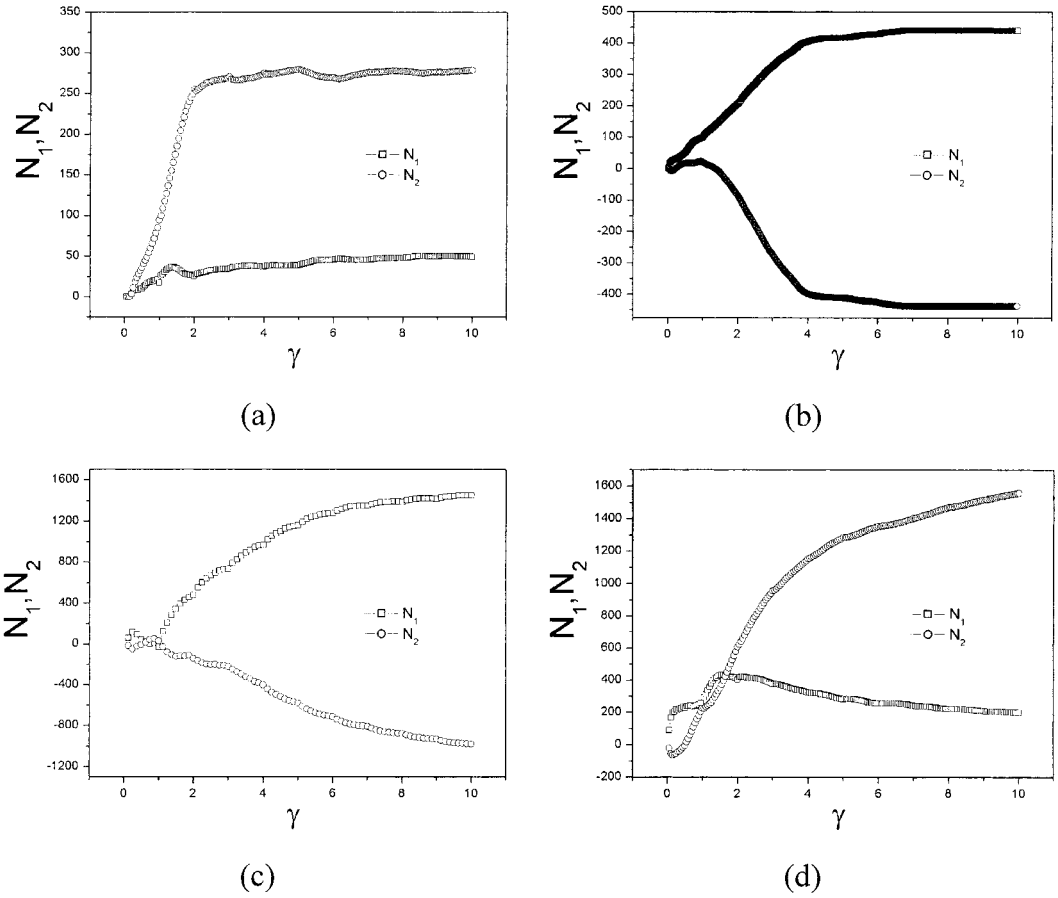

Figure 12. First normal stress difference N_1 and N_2 as a function of strain for (a) $\chi N = 11.0$, $S = 0.001$; (b) $\chi N = 11.0$, $S = 0.0002$; (c) $\chi N = 15.0$, $S = 0.0025$; and (d) $\chi N = 15.0$, $S = 0.001$.

different reduced shear rate, $S = 0.001$ and 0.0002, respectively. Figure 12c,d shows the case of $\chi N = 15.0$ for different reduced shear rate, $S = 0.0025$ and 0.001, respectively. It is clearly seen that N_1 and N_2 are sensitively dependent on the direction of the lamellar alignment. Figure 12b,c corresponds to the case of forming parallel alignment. We can see that $N_1 > 0$, and it increases with the reduced shear strain and keeps constant value when the reduced shear strain is large. On the contrary, $N_2 < 0$, and it decreases with the reduced shear strain and keeps constant value when the reduced shear strain is large. Figure 12a,d corresponds to the case of forming perpendicular alignment. Compared with Figure 12a,d, it is clear that $N_2 > N_1 > 0$, and both the N_1 and N_2 increase with the reduced shear strain before reaching at a constant value.

4. Conclusions

In this paper, we use the time-dependent Ginzburg−Landau (TDGL) approach to investigate the kinetics of lamellar orientation and rheological properties of diblock copolymers under a simple shear flow. Through the numerical simulation, the following conclusions can be drawn.

(1) A high shear rate can induce the perpendicular alignment in the regime of temperatures just below the order−disorder transition (ODT) temperatures. On the other hand, a low shear rate induces the perpendicular alignment first; eventually, the perpendicular alignment is transformed to parallel alignment via undulation instability.

(2) With further decrease of the temperature, a high shear rate produces the parallel alignment, while a low shear rate induces the perpendicular alignment.

(3) The reduced shear viscosity reaches a maximum rapidly at shear strain near one and then decreases. The first and second normal stress difference N_1 and N_2 are related to the lamellar alignment. For the perpendicular alignment, $N_2 > N_1 > 0$, and both the N_1 and N_2 increase with the reduced shear strain until to a constant value. On the other hand, for the parallel alignment, $N_1 > 0$ and N_1 increases and $N_2 < 0$ and N_2 decreases with the reduced shear strain and both N_1 and N_2 keep a constant value when the reduced shear strain is large.

Acknowledgment. This work is subsidized by the Special Funds for Major State Basic Research Projects (G1999064800), NSF of China and The Shanghai Commission of S&T.

References and Notes

(1) Bates, F. S. *Science* **1991**, *251*, 898.
(2) Bates, F. S.; Fredrickson, G. H. *Annu. Rev. Phys. Chem.* **1990**, *41*, 525. Fredrickson, G. H.; Bates, F. S. *Annu. Rev. Mater. Sci.* **1996**, *26*, 501.
(3) Hamley, I. W. *The Physics of Block Copolymers*; Oxford University Press: Oxford, 1998.
(4) Chen, Z.-R.; Kornfield, J. A. *Polymer* **1998**, *39*, 4679.
(5) Winey, K. I.; Patel, S. S.; Larson, R. G.; Watannabe, H. *Macromolecules* **1993**, *26*, 2542.
(6) Winey, K. I.; Patel, S. S.; Larson, R. G.; Watannabe, H. *Macromolecules* **1993**, *26*, 4373.
(7) Patel, S. S.; Larson, R. G.; Winey, K. I.; Watannabe, H. *Macromolecules* **1995**, *28*, 4313.

(8) Pinheriro, B. S.; Hajduk, D. A.; Gruner, S. M.; Winey, K. I. *Macromolecules* **1996**, *29*, 1482.
(9) Polis, D. L.; Winey, K. I. *Macromolecules* **1998**, *31*, 3617.
(10) Gupta, V. K.; Krishnamoorti, R.; Kornfield, J. A.; Smith, S. D. *Macromolecules* **1995**, *28*, 4464.
(11) Gupta, V. K.; Krishnamoorti, R.; Chen, Z.-R.; Kornfield, J. A.; Smith, S. D.; Satkowski, M. M.; Grothous, J. T. *Macromolecules* **1996**, *29*, 875.
(12) Gupta, V. K.; Krishnamoorti, R.; Kornfield, J. A.; Smith, S. D. *Macromolecules* **1996**, *29*, 1359.
(13) Chen, Z.-R.; Kornfield, J. A.; Smith, S. D.; Grothaus, J. T.; Satkowski, M. M. *Science* **1997**, *277*, 1248.
(14) Zhang, Y.; Wiesner, U.; Spiess, H. W. *Macromolecules* **1995**, *28*, 778.
(15) Zhang, Y.; Wiesner, U. *J. Chem. Phys.* **1995**, *103*, 4784.
(16) Zhang, Y.; Wiesner, U.; Yang, Y.; Pakula, T.; Spiess, H. W. *Macromolecules* **1996**, *29*, 5427.
(17) Zhang, Y.; Wiesner, U. *J. Chem. Phys.* **1997**, *106*, 2961.
(18) Maring, D.; Wiesner, U. *Macromolecules* **1997**, *30*, 660.
(19) Koppi, K. A.; Tirrell, M.; Bates, F. S.; Almdal, K.; Colby, R. H. *J. Phys. II* **1992**, *2*, 1941.
(20) Koppi, K. A.; Tirrell, M.; Bates, F. S. *Phys. Rev. Lett.* **1993**, *70*, 1449.
(21) Kannan, R. M.; Kornfield, J. A. *Macromolecules* **1994**, *27*, 1177.
(22) Pinheriro, B. S.; Winey, K. I. *Macromolecules* **1998**, *31*, 4447.
(23) Okamoto, S.; Saijo, K.; Hashimoto, T. *Macromolecules* **1994**, *27*, 5547.
(24) Polis, D. L.; Winey, K. I. *Macromolecules* **1996**, *29*, 8180.
(25) Balsara, N. P.; Hammouda, B.; Kesani, P. K.; Jonnalagadda, S. V.; Straty, G. C. *Macromolecules* **1994**, *27*, 2566.
(26) Zryd, J. L.; Burghardt, W. R. *Macromolecules* **1998**, *31*, 3656.
(27) Kitade, S.; Ochiai, N.; Takahashi, Y.; Noda, I.; Matsushita, Y.; Karim, A.; Nakatani, A. I.; Kim, H.; Han, C. C. *Macromolecules* **1998**, *31*, 8083.
(28) Cates, M. E.; Milner, S. T. *Phys. Rev. Lett.* **1989**, *62*, 1856.
(29) Fredrickson, G. H. *J. Rheol.* **1994**, *38*, 1045.
(30) Zvelindovsky, A. V.; Sevink, G. J. A.; Fraaije, J. G. E. M. *Phys. Rev. E* **2000**, *62*, R3063.
(31) Zvelindovsky, A. V.; Sevink, van Vlimmeren, B. A. C.; G. J. A.; Fraaije, J. G. E. M. *Phys. Rev. E* **1998**, *57*, R4897.
(32) Ohta, T.; Enomoto, Y.; Harden, J. L.; Doi, M. *Macromolecules* **1993**, *26*, 4928.
(33) Doi, M.; Harden, J. L.; Ohta, T. *Macromolecules* **1993**, *26*, 4935.
(34) Ohta, T.; Kawassaki, K. *Macromolecules* **1986**, *19*, 2621.
(35) Ohta, T.; Nozaki, T.; Doi, M. *J. Chem. Phys.* **1990**, *93*, 2664.
(36) Qi, S.; Wang, Z. G. *Phys. Rev. Lett.* **1996**, *76*, 1679.
(37) Qi, S.; Wang, Z. G. *Phys. Rev. E* **1997**, *55*, 1682.
(38) Ren, S. R.; Hamley, I. W. *Macromolecules* **2001**, *34*, 116.
(39) Oono, Y.; Puri, S. *Phys. Rev. A* **1988**, *38*, 434. Puri, S.; Oono, Y. *Phys. Rev. A* **1988**, *38*, 1542.
(40) Shinozaki, A.; Oono, Y. *Phys. Rev. E* **1993**, *48*, 2622.
(41) Kawasaki, K.; Ohta, T. *Physica A* **1986**, *139*, 233.
(42) Corberi, E.; Gonnella, G.; Lamura, A. *Phys. Rev. Lett.* **1999**, *83*, 4057; **1998**, *81*, 3852.
(43) Corberi, E.; Gonnella, G.; Lamura, A. *Phys. Rev. E* **2000**, *61*, 6621.
(44) Luo, K. F.; Yang, Y. L. *J. Chem. Phys.* **2001**, *115*, 2818.
(45) Williams, D. M.; MacKintosh, F. C. *Macromolecules* **1994**, *27*, 7677.
(46) Wang, H.; Kesani, P. K.; Balsara, N. P.; Hammouda, B. *Macromolecules* **1997**, *30*, 982.

MA010889J